A Compact Model for Stochastic Spike-Timing-Dependent Plasticity (STDP) Based on Resistive Switching Memory (RRAM) Synapses

Stefano Bianchi, *Student Member, IEEE*, Giacomo Pedretti, *Student Member, IEEE*, Irene Muñoz-Martín, *Student Member, IEEE*, Alessandro Calderoni, Nirmal Ramaswamy, *Senior Member, IEEE*, Stefano Ambrogio, *Member, IEEE*, and Daniele Ielmini, *Fellow, IEEE*

***Abstract*— Resistive switching memory (RRAM) devices have been proposed to boost the density and the bio-realistic plasticity in neural networks. One of the main limitations to the development of neuromorphic systems with RRAM devices is the lack of compact models for the simulation of spiking neural networks, including neuron spike processing, synaptic plasticity, and stochastic learning. Here, we present a predictive model for neuromorphic networks with unsupervised spike timing-dependent plasticity (STDP) in HfO_2 RRAM devices. Our compact model can predict the learning behavior of experimental networks and can speed up the simulation of unsupervised learning compared to Monte Carlo (MC) approaches. The model can be used to optimize the classification accuracy of data sets, such as MNIST, and to estimate the time of learning and the energy consumption.**

***Index Terms*— Neuromorphic engineering, resistive switching memory (RRAM), spike-timing-dependent plasticity (STDP), stochastic learning, unsupervised learning.**

I. Introduction

THE spiking neural network (SNN) is one of the most suitable ways to perform brain-inspired computing [1]. Learning in the brain takes place via synaptic plasticity, where the synaptic weights are increased or decreased depending on the timing of the spikes being fired from the presynaptic (PRE) and the postsynaptic (POST) neurons. In spike-timing-dependent plasticity (STDP), experimentally observed in the brain [2], [3], weight potentiation takes place when the PRE spike precedes the POST spike while weight depression occurs when the PRE spike follows the POST spike [4]–[6]. Artificial synapses capable of learning via STDP were proposed by using CMOS technology [7], [8] and memristive devices such as resistive switching memory (RRAM) [9]–[13] and phase change memory (PCM) [14]–[17]. STDP was also shown to be fundamental to achieve energy-efficient continual learning in artificial neural networks (ANNs) [18], [19].

However, despite these achievements, unsupervised learning via synaptic plasticity at the network level is still an open challenge. Stochastic training has been proposed to support unsupervised learning by STDP [12], [20], although the impact of the density and frequency of pattern and stochastic noise presentation has only been partially explored. The design of neuromorphic circuits for STDP-based unsupervised learning is usually addressed by Monte Carlo (MC) simulations, which easily handle the stochastic spiking activities of the RRAM synapses [12] but suffer from excessive computational time.

This article introduces an analytical framework for unsupervised learning by STDP with RRAM synapses, starting from theoretical rules [21], [22]. Based on rate equations of the synaptic weights in the network, the model allows to predict the learning speed and energy efficiency as a function of the learning parameters, such as the pattern density or the noise rate of submission. The compact tool thus provides fast design and optimization of the algorithms for unsupervised learning [23]. We also demonstrate that the model is robust and flexible versus device nonidealities, and it can describe other types of memory devices used as synaptic elements, like PCMs.

II. STDP Network

A. Experimental Study

Fig. 1(a) illustrates a scheme of a one-layer SNN with N_{PRE} PREs and one POST. The network is fully connected

Manuscript received March 21, 2020; accepted April 28, 2020. Date of publication May 20, 2020; date of current version June 19, 2020. This work was supported in part by the European Research Council (ERC) under the European Union's Horizon 2020 Research and Innovation Program under Grant 648635 and in part by the Italian Minister for University and Research under Grant R164TYLBZP. The review of this article was arranged by Editor B. K. Kaushik. *(Corresponding author: Daniele Ielmini.)*

Stefano Bianchi, Giacomo Pedretti, Irene Muñoz-Martín, and Daniele Ielmini are with the Dipartimento di Elettronica, Informazione e Bioingegneria and Italian Universities Nanoelectronics Team, Politecnico di Milano, 20133 Milan, Italy (e-mail: stefano1.bianchi@polimi.it; giacomo.pedretti@polimi.it; irene.munoz@polimi.it; daniele.ielmini@polimi.it).

Alessandro Calderoni and Nirmal Ramaswamy are with Micron Technology, Inc., Boise, ID 83707 USA (e-mail: acaldero@micron.com; dramaswamy@micron.com).

Stefano Ambrogio was with the Dipartimento di Elettronica, Informazione e Bioingegneria, Politecnico di Milano, 20133 Milan, Italy. He is now with IBM Research-Almaden, San Jose, CA 95120 USA (e-mail: stefano.ambrogio@ibm.com).

Color versions of one or more of the figures in this article are available online at http://ieeexplore.ieee.org.

Digital Object Identifier 10.1109/TED.2020.2992386

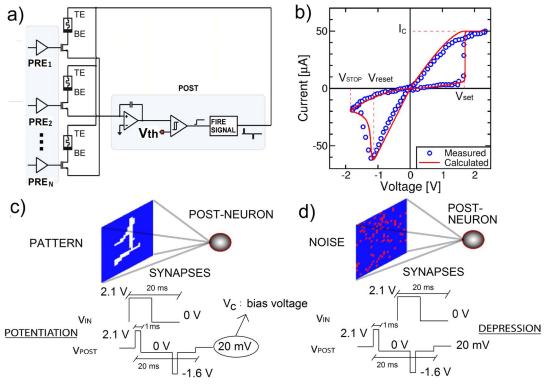

Fig. 1. (a) Schematic of a SNN with several preneurons connected to one POST by 1T1R synapses implementing the STDP protocol. (b) Measured and calculated *I*–*V* curves of the RRAM device used in this article. (c) Illustration of synaptic potentiation following pattern presentation due to STDP at positive delay. (d) Illustration of synaptic depression following noise presentation due to STDP at negative delay.

since there is one synapse between each PRE and the POST. The synapses have a 1T1R structure, where the synaptic gate is connected to the PRE that generates the characteristic input spike, while the top electrode (TE) and the bottom electrode (BE) are connected to the POST [20], [23]. Fig. 1(b) shows the I–V characteristics of the typical 1T1R RRAM synapse, indicating the set voltage V_{set}, the reset voltage V_{reset}, and the stop voltage V_{STOP}. The gate voltage is generally biased to induce a maximum current I_C across the RRAM during set, thus enabling the control of the resistance. The application of a PRE spike to the synaptic gate induces a current flow through the RRAM device, which is collected and integrated by the internal potential V_{int} of the POST. As V_{int} reaches the threshold, it fires, sending a feedback spike to all the TE of synapses connected to it. The feedback spike consists of a positive pulse of voltage $V_{\text{TE+}} > V_{\text{set}}$, followed by a negative pulse of voltage $V_{\text{TE–}} < V_{\text{reset}}$. The overlap between the PRE spike and the POST spikes induces potentiation (set transition) or depression (reset) for positive or negative delay between the two spikes [12]. The stochastic presentation of a pattern and noise to the PRE channels, results in potentiation [i.e., low resistive state (LRS)] of the pattern synapses, namely, those located at pattern pixels, and depression [i.e., high resistive state (HRS)] of background synapses, namely all the other synapses [20]. The different effects on pattern and background synapses are due to the time correlation of the pattern spikes. As a result, the presentation of the pattern is likely followed by a POST fire, satisfying the STDP rule for potentiation [Fig. 1(c)]. On the other hand, noise hardly induces POST fires, rather it may induce depression due to STDP when it is submitted soon after a fire event [Fig. 1(d)]. The stochastic submission of pattern and random uncorrelated noise thus leads to unsupervised learning of the pattern, irrespective of the initial configuration of synaptic weights [20].

Fig. 2(a) shows the experimental setup, with the RRAM synapses connected to the CMOS neurons and to Arduino. Fig. 2(b) shows the synaptic evolution of an

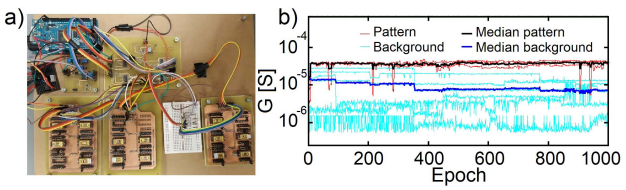

Fig. 2. (a) Experimental setup with RRAM synapses, CMOS neurons and an Arduino microcontroller as a control logic. (b) Measured conductances of the 1T1R synapses as a function of time under STDP learning activity.

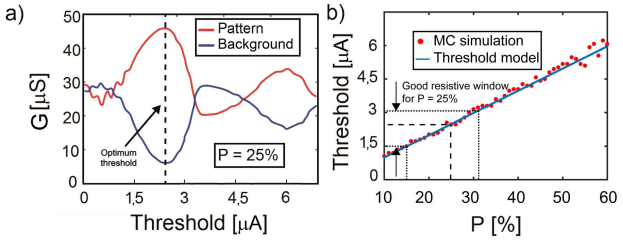

Fig. 3. (a) MC simulations in a SNN with 16 PREs and 1 POST of the average conductance for pattern synapses and background synapses at the end of stochastic learning with 500 epochs. (b) Optimized threshold as a function of the pattern density *P*.

STDP-based learning activity. The depression is slow and gradual compared to potentiation due to the uncorrelated nature of noise that acts randomly on background synapses, while potentiation occurs after the very first pattern submission [20].

B. MC Simulations

MC simulations are the most suitable for the prediction of the SNN performance during stochastic unsupervised learning. The MC model can also describe the variable switching of the RRAM devices, which plays an important role for the synaptic weights. Although the MC simulations show a good agreement with experimental data, several time-consuming simulations (e.g., 1000) are needed to yield the average behavior of the synaptic weights in the pattern and background.

C. Threshold Optimization

The fire threshold of the POST should be carefully set to get the maximum resistive window between pattern and background synapses. In the following, we will refer to the current directly coming from the synapses, in order to be independent of the effective POST realization. Fig. 3(a) reports the MC results of the average pattern/background conductances as a function of the threshold for a fixed pattern density ($P = 25\%$), after 500 epochs. The conductance window shows a maximum for $I_{\text{th}} \approx 2.1\ \mu$A, corresponding to a single submission of the pattern with 53% of the full LRS conductance G_{LRS}. The pattern conductance shows a periodic behavior where the first peak, at the optimum threshold, corresponds to a fire with one single submission, whereas the second peak corresponds to a fire with two sequential submissions of the pattern. The peak of the background conductance corresponds instead to the fire event after the submission of

a pattern and a consequent noise presentation. Fig. 3(b) shows the position of the optimum threshold as a function of the pattern density P. A good resistive window with $P = 25\%$ is achievable even for different pattern densities, thus avoiding any peripheral circuit for adapting the threshold. The results of the MC simulations can be linearly fit by the formula

$$I_{\text{th}} = K V_C G_{\text{LRS}} P N_{\text{PRE}} \tag{1}$$

where $K = 0.53$, V_C is the read bias voltage at the TE inducing the current spike, G_{LRS} is the maximum conductance, and N_{PRE} the total number of pixels in the PRE channels.

III. Compact Model of STDP Learning

The goal of the model is to analytically describe the time evolution of pattern and background average synaptic weights depending on the stochastic variables of unsupervised STDP, such as the densities and rates of pattern and noise signals. The evolution is described as a dynamic equilibrium between forces, arising from the external PRE stimulation that causes either synaptic potentiation or depression. The presentation of the pattern causes the potentiation of the average synaptic weights in the pattern region, namely G_p. The model describes the time evolution of G_p by the rate equation

$$\frac{dG_p}{dt} = ANR_N(G_{\text{LRS}} + G_{\text{HRS}} - 2G_p) + C(G_{\text{LRS}} - G_p)(G_p - \alpha N G_{\text{HRS}})(p - n)R_P \tag{2}$$

where A, C, and α are constants related to the STDP algorithm with an epoch duration of 10 ms, N is the noise density given by the average number of noise pixels divided by N_{PRE}, G_{HRS} is the minimum conductance, R_P and R_N are the pattern/noise probabilities, namely the average occurrence of pattern/noise presentation with respect to all presentations. Similarly, the time evolution of the average synaptic weight in the background, namely G_b, is described by the rate equation

$$\frac{dG_b}{dt} = A'NR_N(G_{\text{LRS}} + G_{\text{HRS}} - 2G_b) + D(\beta G_{\text{LRS}} - G_b)(G_b - G_{\text{HRS}})(N - P)R_N R_P \frac{NB}{B + P} \tag{3}$$

where A', D, and β are constants related to the STDP algorithms with an epoch duration of 10 ms. Table I summarizes variables and parameters entering (2) and (3).

Note that (2) and (3) describe the behavior of a network of synapses not a specific RRAM device. The only physical parameters that depend on the device are the maximum and minimum conductances, namely G_{LRS} and G_{HRS}, respectively. In addition, the switching time is assumed to be much faster than the typical neuron spike time, so that a single spike applied to a RRAM synapse is capable of inducing a full potentiation (set transition), or depression (reset transition).

Both equations have two terms on the right-hand side, where the first term describes the random equalization of weights induced by the noise. Noise is a random parameter of the STDP learning activity with a uniform probability (given by N) of falling in any position of the input neuron array. In fact, if only noise is submitted, both G_p and G_b randomly

TABLE I
VARIABLES AND PARAMETERS ENTERING THE COMPACT MODEL

VARIABLE	DEFINITION
P	Pattern density
B	Background density
N	Noise density
R_P	Pattern probability
R_N	Noise probability

PARAMETER	VALUE
A	10 s^{-1}
A'	0.5 s^{-1}
C	R_p*30*10^5 Ωs^{-1}
D	R_p*35*10^6 Ωs^{-1}
α	60
β	0.69
G_{HRS}	(300 kΩ)$^{-1}$
G_{LRS}	(20kΩ)$^{-1}$

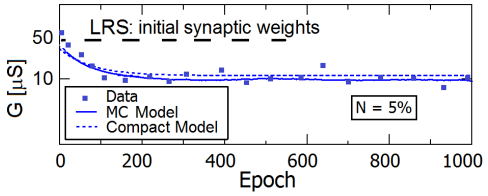

Fig. 4. Measured and calculated synaptic weights as a function of time for stochastic learning with purely random noise spikes for noise density $N = 5\%$ and LRS starting condition for all the 16 synapses. Calculations from both the MC model and the compact model are shown. The final average conductance is intermediate between HRS and LRS nominal values.

fluctuate, yielding an equalized average conductance between HRS and LRS, namely $(G_{\text{HRS}} + G_{\text{LRS}})/2$. To reflect the role of noise as the driving force for equalization, the first term is proportional to N and R_N. The effect of noise is shown in Fig. 4, indicating experimental data compared to MC and model simulations of random weight potentiation/depression under the submission of noise spikes. The average G_p and G_b remain almost constant close to the average conductance between LRS and HRS. The second term in (2) represents the potentiation of pattern synapses in response to pattern spikes. A fire event in response to pattern presentation results in pattern weight potentiation and background weight depression, whereas a fire event in response to the presentation of noise would lead to pattern depression and background potentiation, which explains the proportionality of the second term to p-n in (2) and to n-p in (3).

Note that the potentiation rate in (2) is proportional to R_P, as the presentation of the pattern leads to both PRE spikes and the responding POST fire [Fig. 1(c)]. On the other hand, the depression rate in (3) is proportional to both R_P and R_N, as the PRE spikes are controlled by R_N, whereas the POST spikes are controlled by R_P [Fig. 1(d)].

The pattern weight saturates as it approaches G_p, thus the potentiation rate in (2) is proportional to $G_{\text{LRS}} - G_p$. Similarly, the depression rate in (3) is proportional to $G_b - G_{\text{HRS}}$, to allow for saturation of G_b as it approaches G_{HRS} at sufficiently long time. These boundaries occur for a standard stochastic learning operation, that is, for $P > N$. On the other hand, for unconventional operation of the network with $N > P$, G_p saturates at $\alpha N G_{\text{HRS}}$, whereas G_b saturates at βG_{LRS}, which is taken into account in (2) and (3), respectively. The parameters α and β are obtained as fitting parameters from the comparison with the MC simulations.

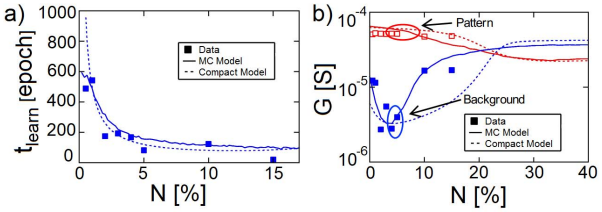

Fig. 5. Measured and calculated (a) t_{learn} and (b) G_p and G_b as a function of noise density N. Calculations by both the MC model and the compact model are shown. All results were collected after 1000 epochs. We used pattern density $P = 25\%$ and input pattern/noise probabilities $R_P = R_N = 50\%$. The best tradeoff between learning speed and accuracy is at $N \approx 3\%$.

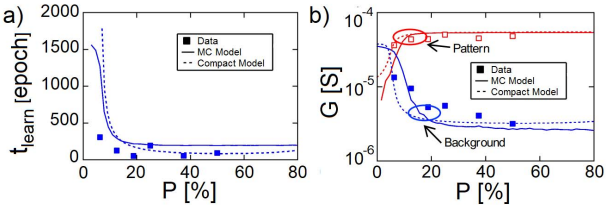

Fig. 6. Measured and calculated (a) t_{learn} and (b) G_p and G_b as a function of pattern density P. Calculations by both the MC model and the compact model are shown. A noise density $N = 3\%$ and pattern/noise probabilities $R_P = R_N = 50\%$ were assumed. Stable learning takes place for $P \gg N$.

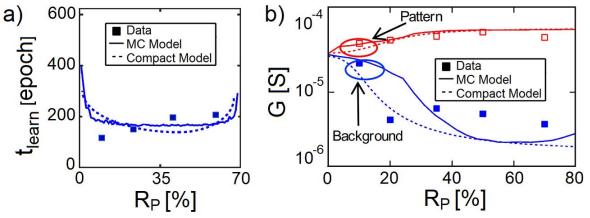

Fig. 7. Measured and calculated (a) t_{learn} and (b) G_p and G_b as a function of input pattern probability of appearance R_P with noise probability $R_N = 1 - R_P$. A noise density $N = 3\%$ and pattern density $P = 25\%$ were assumed.

IV. Results

The purpose of our model is the prediction of the synaptic weights during unsupervised learning for various spiking stimulation affecting potentiation and depression, such as the signal densities (P and N) and probabilities (R_P and R_N) of pattern and noise presentation, respectively. Equations (2) and (3) can be used to predict the performance of an SNN such as the magnitude of the learning window, $G_p - G_b$, and the learning time. The learning window should be maximized for best separation of pattern and background synapses after 1000 epochs. The learning time t_{learn} is the time needed for depression of the background synapses below a conductance of 15 μs. This figure of merit is due to the fact that background depression is generally slower than pattern potentiation.

Simulation results from the compact model and the MC model were compared to experimental data for a perceptron-type SNN with 16 PRE fully connected to a single POST [20]. Every data point was obtained as the average among five experiments conducted on a hardware SNN with 1T1R RRAM synapses [20]. MC simulations were repeated 1000 times to assess the average value.

A. Dependence on Noise Density N

Fig. 5 shows the measured and calculated t_{learn} [Fig. 5(a)] and synaptic weights G_p and G_b [Fig. 5(b)] as a function of the noise density N. The stochastic learning session was 1000 epochs long, and the submitted pattern had a density $P = 25\%$. The learning time decreases at increasing N due to the enhanced depression rate in (3) at high N. Fig. 5(b) shows that the conductance window is relatively large at low N, with an optimum learning window for $N \approx 3\%$, as evident from MC simulations. For lower values of N no full depression of the background can be attained as the learning time is too long. For larger values of N, approaching the pattern density P, instability effects occur for both the pattern and the background synapses, leading to a window closure and degraded learning. Both the MC model and the compact model predict an inversion of synaptic weights for N exceeding P.

B. Dependence on Pattern Density P

Fig. 6 shows the measured and calculated t_{learn} [Fig. 6(a)] and the average synaptic conductance G_p and G_b [Fig. 6(b)] as a function of P. Based on Fig. 5, we adopted an average noise density $N = 3\%$ in the experiments and calculations. The learning time decreases with P, since the background size increases for P close to 0, thus the time required for background depression at a given N increases. The synaptic conductance in Fig. 6(b) shows that the learning window is relatively low for P comparable or smaller than N. As P increases, the window reaches a large value, indicating stable learning. The results confirm the relevance of the competition between pattern and noise, which requires $P \gg N$ for stability.

C. Dependence on Pattern Rate R_P and Noise Rate R_N

Fig. 7 shows the measured and calculated t_{learn} [Fig. 7(a)] and the average synaptic conductance G_p and G_b [Fig. 7(b)] as a function of R_P increasing from 0% to 80%, with $R_N = 1 - R_P$. The learning time first decreases at increasing R_P, then slightly increases. The optimum condition is found for $R_N = R_P$, which maximizes the product $R_N * R_P$ in (3) for the background depression. The average conductance in Fig. 7(b) reaches the best window for relatively large R_P.

D. Flexibility and Robustness

We tested our model for other synaptic devices, like PCMs, and the robustness against device nonidealities, such as a limited switching time and LRS/HRS variations.

Fig. 8(a) shows the PCM distributions for LRS and HRS. Compared to HfO_2 RRAM, the resistive window is larger, approaching two orders of magnitude [16]. We first ran MC simulations and then tested the prediction capability of the compact model by adapting G_{LRS} and G_{HRS} according to the PCM distributions. All other parameters were kept constant. Fig. 8(b)–(d) shows the fitting of the compact model versus

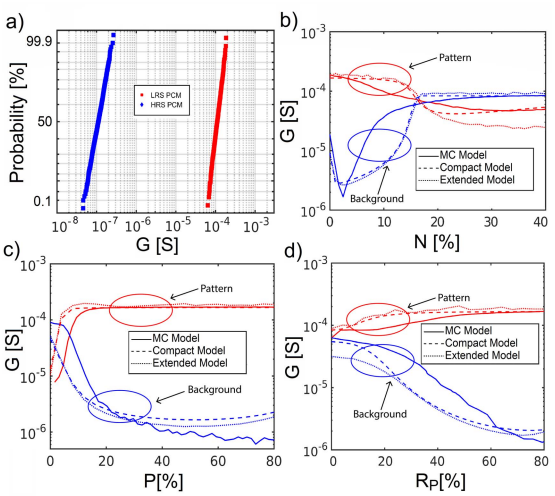

Fig. 8. (a) Distributions of LRS and HRS values fo the PCM device. Calculated G_p and G_b as a function of (b) N, (c) P, and (d) R_P. The optimum operation is found at low N, $N \approx 3\%$, and at high R_P, $R_P \approx 60\%$. The dashed-dot lines show the tendencies of the model when the statistical distributions for LRS and HRS are taken into consideration in the equations.

MC simulations for the average synaptic conductances G_p and G_b as a function of N, P, and R_P, respectively. Concerning the switching time, it comes out that the variations are not a problem because the bio-inspired reference time for STDP is slow [Fig. 1(c) and (d)] compared to the device worst case switching time ($\approx$100 μs for HfO_2 RRAMs); on the other hand, the conductance variations directly affect (2) and (3). To stress this point, we extracted a set of G_{LRS} and G_{HRS} values from PCM distributions aiming to statistically describe the time evolution of the average synapse of the experimental setup (16 PREs, 1 POST). The extended model was tested to predict the average synaptic conductances G_p and G_b as a function of N, P, and R_P, respectively. The tendencies are represented by the short-dashed lines in Fig. 8(b)–(d), showing consistency respect to MC calculations.

E. Impact on Learning Efficiency

To evaluate the learning efficiency, we measured P_{learn} and P_{err}, namely the probabilities of POST fire in response to the submission of the true pattern and the error in response to a submission of a false pattern with the same P, respectively [23]. To extend the compact model to the statistical study, we assumed the relationship between the average conductance and its standard deviation obtained by experimental distributions of HfO_x RRAMs [12]. Fig. 9(a)–(c) shows the measured P_{learn} and P_{err} as a function of N, P, and R_P, respectively, compared with calculations from the MC and the compact models.

V. Model-Based Optimization of Learning

The compact model of (2) and (3) can be used to optimize the stochastic STDP learning algorithm. To illustrate the optimization methodology, Fig. 10(a) shows the contour plot of t_{learn} calculated with the compact model as a function of

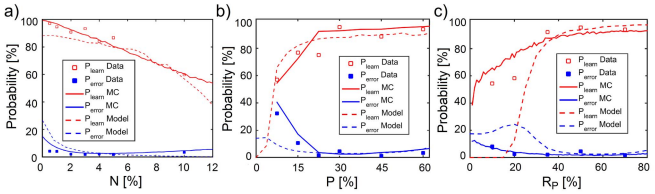

Fig. 9. Measured and calculated P_{learn} and P_{err} as a function of (a) noise density N, (b) pattern density P, and (c) pattern probability R_P, with $R_N = 1 - R_P$. P_{learn} is the probability of POST fire in response to the true pattern, i.e., the one used for training; P_{err} is the probability of fire in response to the presentations of false patterns with the same P but different shapes.

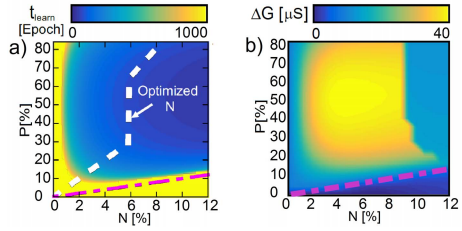

Fig. 10. (a) Contour plot of the calculated t_{learn} obtained from the compact model as a function of P and N. The white line shows the values of N which maximize the learning window. (b) Contour plot of the calculated learning window $G_p - G_b$ from the compact model as a function of P and N. The dashed-dotted lines indicate the region $P < N$, where learning cannot converge.

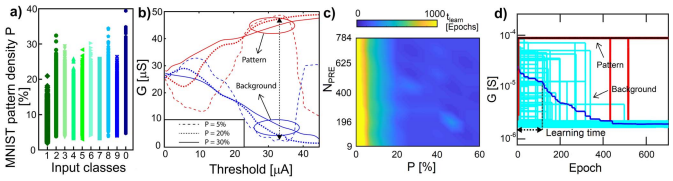

Fig. 11. (a) Pattern densities per class in the MNIST data set are between 3% and 35%. (b) However, there is a single threshold value capable of providing a good resistive window between pattern and background average synapses. Color map of the MC simulations for t_{learn} as a function of P and the input size N_{PRE}, from a 3×3 to a 28×28 pattern. (c) Note that t_{learn} depends on P but not on the dimensions of the input. (d) Learning activity of an MNIST image showing the evolution of the synaptic weights.

P and N for HfO_2 RRAM synapses. Note that every stable learning requires $N \ll P$ (region above the red dashed line). It is possible to identify an "optimized N" which maximizes the learning window ΔG, as reported in Fig. 10(b).

A. Estimation of t_{learn} and Minimum Energy Consumption for MNIST Images

To test the scalability of the model, we simulated the unsupervised learning of 60 000 independent handwritten digits from the MNIST training data set. Note that the pattern density of MNIST data set ranges from 3% to over 30%, as shown in Fig. 11(a). This raises the issue of identifying a unique unsupervised threshold for all the 60 000 learning activities. To this purpose, MC simulations in Fig. 11(b) confirm that the STDP learning methodology can operate with a single threshold $I_{TH} = 35$ μA for a wide range of P, thus avoiding the need of any peripheral adaptive circuit.

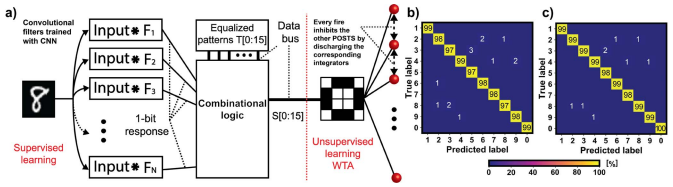

Fig. 12. (a) Block scheme of a mixed supervised–unsupervised neural network, with trained convolutional filters and WTA STDP. (b) Confusion matrix for the standard results of full MNIST testing [19]. (c) Confusion matrix of the optimized learning procedure enabled by the use of the compact model.

The STDP algorithm is scalable, as the learning time and window is independent of the effective size of the input pattern. This is demonstrated in Fig. 11(c), showing a color map of the learning time obtained from MC simulations as a function of pattern size N_{PRE} and density P. The learning time is approximately constant for each P irrespective of N_{PRE}. Similar results were obtained for the learning window ΔG.

The learning time can be evaluated from the compact model, Fig. 10(a). Assuming a bio-compatible epoch of 10 ms, a learning time of 2.5 s (i.e., 250 epochs) is obtained. Fig. 11(d) shows the MC simulations of a fast learning activity of an MNIST digit and the corresponding synaptic evolutions in time. By reducing the time of each epoch, it is possible to achieve a faster response of the network per single image [18].

The compact model can also predict the average energy consumption for the learning of an MNIST image. The energy includes two contributions, namely fire and integration. The energy required by the single synapse for firing is $E_{\mathrm{fire}} = I_{\mathrm{set/reset}} \times V_{\mathrm{set/reset}} \times t_{\mathrm{fire}}$, while for integrating is $E_{\mathrm{int}} = G_{\mathrm{LRS/HRS}} \times V_{\mathrm{read}}{}^2 \times t_{\mathrm{int}}$. Considering the model estimations for which the fire occurs at every pattern presentation ($R_P = 50\%$), assuming an average t_{learn} of 250 epochs from Fig. 10(a), an average P for MNIST from Fig. 11(a), and the setup values of Fig. 1, we estimate the minimum energy required for learning a single MNIST image to be in the range of 3 mJ.

B. Improvement of the MNIST Classification

Unsupervised learning based on STDP is a robust technique for achieving accurate continual learning when introduced in the last layer of a convolutional neural network (CNN) [18], [19]. These supervised/unsupervised networks rely on custom training algorithms to extract, after convolution, a single-bit response relative to a found/not found trained feature, as illustrated in Fig. 12(a). A combinational logic equalizes the response of the CNN filters to ensure a fixed-density pattern as input to the winner-take-all (WTA) unsupervised network. The WTA network consists of ten POSTs with inhibitory signals, where a neuron that fires induces the drop of the internal potential in all other neurons [20]. Our compact model can optimize the accuracy of the mixed supervised–unsupervised network acting on the unsupervised STDP. Since the equalized patterns are partially overlapping one to each other, we chose $P = 40\%$ to increase P_{learn} and to reduce P_{err}, according to Fig. 9. Furthermore, to speed up the learning process and maximize the learning window ΔG, we selected $N = 6\%$, from Fig. 10, and $R_P = 60\%$. The optimization provided by the compact model allows a significant improvement ($\approx$1%) for the full testing accuracy of the MNIST data set, as evident by the comparison between the confusion matrices of Fig. 12(b) and (c), thus highlighting the relevance of the compact model for the design of unsupervised learning networks.

VI. Conclusion

A compact model describing unsupervised learning in SNN based on biological plasticity rules, as the STDP, has been shown. Results of the model have been tested against experimental data and MC simulations as a function of the parameters controlling the learning process. The model can estimate and optimize SNNs for fast and efficient learning, like the case of unsupervised learning of the MNIST data set. The model provides a valuable tool and methodology toward the development and optimization of SNNs capable of information processing and learning similar to the human brain.

References

[1] W. Maass, "Networks of spiking neurons: The third generation of neural network models," *Neural Netw.*, vol. 10, no. 9, pp. 1659–1671, 1997, doi: 10.1016/S0893-6080(97)00011-7.

[2] G.-Q. Bi and M.-M. Poo, "Synaptic modifications in cultured hippocampal neurons: Dependence on spike timing, synaptic strength, and postsynaptic cell type," *J. Neurosci.*, vol. 18, no. 24, pp. 10464–10472, Dec. 1998, doi: 10.1523/JNEUROSCI.18-24-10464.1998.

[3] L. F. Abbott and S. B. Nelson, "Synaptic plasticity: Taming the beast," *Nature Neurosci.*, vol. 3, no. S11, pp. 1178–1183, Nov. 2000, doi: 10.1038/81453.

[4] P. U. Diehl and M. Cook, "Unsupervised learning of digit recognition using spike-timing-dependent plasticity," *Frontiers Comput. Neurosci.*, vol. 9, p. 99, Aug. 2015, doi: 10.3389/fncom.2015.00099.

[5] T. Masquelier and S. J. Thorpe, "Unsupervised learning of visual features through spike timing dependent plasticity," *PLoS Comput. Biol.*, vol. 3, no. 2, pp. 247–257, Feb. 2007, doi: 10.1371/journal.pcbi.0030031.

[6] W. Maass, "Noise as a resource for computation and learning in networks of spiking neurons," *Proc. IEEE*, vol. 102, no. 5, pp. 860–880, May 2014, doi: 10.1109/JPROC.2014.2310593.

[7] E. Chicca, F. Stefanini, C. Bartolozzi, and G. Indiveri, "Neuromorphic electronic circuits for building autonomous cognitive systems," *Proc. IEEE*, vol. 102, no. 9, pp. 1367–1388, Sep. 2014, doi: 10.1109/JPROC.2014.2313954.

[8] G. Indiveri and S.-C. Liu, "Memory and information processing in neuromorphic systems," *Proc. IEEE*, vol. 103, no. 8, pp. 1379–1397, Aug. 2015.

[9] S. H. Jo, T. Chang, I. Ebong, B. B. Bhadviya, P. Mazumder, and W. Lu, "Nanoscale memristor device as synapse in neuromorphic systems," *Nano Lett.*, vol. 10, no. 4, pp. 1297–1301, Apr. 2010, doi: 10.1021/nl904092h.

[10] H.-S.-P. Wong *et al.*, "Metal–oxide RRAM," *Proc. IEEE*, vol. 100, no. 6, pp. 1951–1970, Jun. 2012, doi: 10.1109/JPROC.2012.2190369.

[11] S. Yu, Y. Wu, R. Jeyasingh, D. Kuzum, and H.-S.-P. Wong, "An electronic synapse device based on metal oxide resistive switching memory for neuromorphic computation," *IEEE Trans. Electron Devices*, vol. 58, no. 8, pp. 2729–2737, Aug. 2011, doi: 10.1109/TED.2011.2147791.

[12] S. Ambrogio *et al.*, "Neuromorphic learning and recognition with one-transistor-one-resistor synapses and bistable metal oxide RRAM," *IEEE Trans. Electron Devices*, vol. 63, no. 4, pp. 1508–1515, Apr. 2016, doi: 10.1109/TED.2016.2526647.

[13] M. Prezioso *et al.*, "Spike-timing-dependent plasticity learning of coincidence detection with passively integrated memristive circuits," *Nature Commun.*, vol. 9, no. 1, p. 5311, Dec. 2018, doi: 10.1038/s41467-018-07757-y.

[14] D. Kuzum, R. G. D. Jeyasingh, B. Lee, and H.-S.-P. Wong, "Nanoelectronic programmable synapses based on phase change materials for brain-inspired computing," *Nano Lett.*, vol. 12, no. 5, pp. 2179–2186, May 2012, doi: 10.1021/nl201040y.

[15] S. Kim *et al.*, "NVM neuromorphic core with 64k-cell (256-by-256) phase change memory synaptic array with on-chip neuron circuits for continuous *in-situ* learning," in *IEDM Tech. Dig.*, Dec. 2015, pp. 443–446, doi: 10.1109/IEDM.2015.7409716.

[16] S. Raoux, W. Wełnic, and D. Ielmini, "Phase change materials and their application to nonvolatile memories," *Chem. Rev.*, vol. 110, no. 1, pp. 240–267, Jan. 2010, doi: 10.1021/cr900040x.

[17] S. Yu, "Neuro-inspired computing with emerging nonvolatile memorys," *Proc. IEEE*, vol. 106, no. 2, pp. 260–285, Feb. 2018, doi: 10.1109/JPROC.2018.2790840.

[18] S. Bianchi, I. Munoz-Martin, G. Pedretti, O. Melnic, S. Ambrogio, and D. Ielmini, "Energy-efficient continual learning in hybrid supervised-unsupervised neural networks with PCM synapses," in *Proc. Symp. VLSI Technol.*, Jun. 2019, pp. T172–T173, doi: 10.23919/VLSIT.2019.8776559.

[19] I. Munoz-Martin, S. Bianchi, G. Pedretti, O. Melnic, S. Ambrogio, and D. Ielmini, "Unsupervised learning to overcome catastrophic forgetting in neural networks," *IEEE J. Explor. Solid-State Comput. Devices Circuits*, vol. 5, no. 1, pp. 58–66, Jun. 2019, doi: 10.1109/JXCDC.2019.2911135.

[20] G. Pedretti *et al.*, "Memristive neural network for on-line learning and tracking with brain-inspired spike timing dependent plasticity," *Sci. Rep.*, vol. 7, no. 1, p. 5288, Dec. 2017, doi: 10.1038/s41598-017-05480-0.

[21] C. Clopath and W. Gerstner, "Voltage and spike timing interact in STDP—A unified model," *Frontiers Synaptic Neurosci.*, vol. 2, p. 25, Jul. 2010, doi: 10.3389/fnsyn.2010.00025.

[22] S. Song, K. D. Miller, and L. F. Abbott, "Competitive Hebbian learning through spike-timing-dependent synaptic plasticity," *Nature Neurosci.*, vol. 3, no. 9, pp. 919–926, Sep. 2000, doi: 10.1038/78829.

[23] G. Pedretti, S. Bianchi, V. Milo, A. Calderoni, N. Ramaswamy, and D. Ielmini, "Modeling-based design of brain-inspired spiking neural networks with RRAM learning synapses," in *IEDM Tech. Dig.*, Dec. 2017, pp. 1–28, doi: 10.1109/IEDM.2017.8268467.